Correlations among Morphology, β-Sheet Stability, and Molecular Structure in Prion Peptide Aggregates†

Sarah A. Petty, Thorsteinn Adalsteinsson, and Sean M. Decatur*

Department of Chemistry, Mount Holyoke College, 50 College Street, South Hadley, Massachusetts 01075

Received December 6, 2004; Revised Manuscript Received January 14, 2005

ABSTRACT: The misfolding of proteins into β-sheets and the subsequent aggregation of these sheets into fibrous networks underlies many diseases. In this paper, the role of peptide structure in determining the ordering of β-sheet aggregates and the morphology of fibrils and protofibrils is dissected. Using a series of peptides based on residues 109−122 of the Syrian hamster prion protein (H1) with a range of substitutions at position 117, the link between side chain interactions and β-sheet thermal stability has been investigated. The thermal stability of β-sheets is associated with the peptides' ability to adopt the same alignment as wild-type H1, with residue 117 in register across all β-strands [Silva, R. A. G. D., Barber-Armstrong, W., and Decatur, S. M. (2003) *J. Am. Chem. Soc. 125*, 13674−13675]. These aligned strands are capable of forming long, rigid, and twisted fibrils (as visualized by atomic force microscopy) which are thermostable. Peptides which do not adopt this strand alignment aggregate to form thin, flexible, and smooth protofibrils. The ability to form ordered aggregates, and thus to form twisted fibrils, is modulated by the structure of the side chain of residue 117.

Protein aggregation, once ignored as an unproductive side reaction of the protein folding pathway, is now recognized as an important biological process. Protein misfolding into fibrous protein aggregates has been inextricably linked with diseases such as Alzheimer's disease, Huntington's disease, and the spongiform encephalopathies (*1*−*3*), and the ability to form ordered, fibrous aggregates may be a generic feature of proteins (*4*). However, the structural details of these aggregates, as well as the mechanism of aggregation, are not fully understood.

The general morphological features of protein aggregates can be imaged by transmission electron microscopy (TEM)[1] or atomic force microscopy (AFM) and can be classified into four morphological categories: amorphous aggregates, which lack any regular long-distance order, protofibrils, thin (∼2−5 nm), flexible assemblies, fibrils, rigid and twisted assemblies, made up of two or more protofibrils, and fibers, dense assemblies of fibrils (*5*−*9*). In several peptide systems, these species are capable of interconversion, with the protofibril and fibril forms serving as intermediates to fibrous amyloid formation. Evidence from spectroscopic techniques (such as circular dichroism, infrared (IR), and solid-state NMR spectroscopies) and X-ray fiber diffraction indicates that the polypeptide backbone adopts a β-sheet conformation within the ordered aggregates (*10*−*16*). However, there is little detailed information on the relationship between the structure and organization of the β-sheets and the aggregate morphology.

In this paper, we present results from isotope-edited IR spectroscopy and AFM studies which correlate β-sheet structure, aggregate stability, and aggregate morphology for a series of peptides based on residues 109−122 of the Syrian hamster prion protein (H1). Misfolding and aggregation of the prion protein (PrP) is associated with the spongiform encephalopathies, including in humans the neurodegenerative diseases Creutzfeldt−Jakob disease (CJD), Gerstmann−Sträussler−Scheinker (GSS) syndrome, and fatal familial insomnia (FFI) (*1*, *17*). Short peptides derived from PrP aggregate to form amyloid fibers in vitro. H1, containing what is believed to be the most amyloidogenic region of PrP (*12*), has been used as a model for characterizing the structure and assembly of β-sheet aggregates (*12*, *13*, *18*). A previous isotopic labeling FTIR study (*18*) has shown that in a 1:1 acetonitrile/water solution, the hydrophobic core of H1 (residues 112−122) forms an antiparallel β-sheet conformation, resulting in the alignment of residue 117 in all of the strands and leaving the first three hydrophilic residues (109−111) as a dangling tail (Figure 1) (*18*). This alignment was derived from the large (∼10 cm^{-1}) shift in the ^{13}C amide I′ band when the backbone carbonyl of residue 117 is labeled with ^{13}C. This shift is indicative of strong transition dipole coupling at this position, which is only possible if the antiparallel β-sheet is organized such that residue 117 is aligned in all of the strands (Figure 1B). To determine the significance of residue 117 in the stability and alignment of the β-sheet within the aggregates, we have synthesized a series of peptides based on H1 in which A117 is replaced with both naturally occurring and synthetic amino acids. Using variable-temperature isotope-edited IR spectroscopy,

† This work was supported by grants from the National Science Foundation (RUI 0415878 and NUE 0407117) and the National Institutes of Health (R15GM54334) and a Henry Dreyfus Teacher-Scholar Award.

* To whom correspondence should be addressed. Fax: (413) 538-2327. Phone: (413) 538-2115. E-mail: sdecatur@mtholyoke.edu.

[1] Abbreviations: IR, infrared; AFM, atomic force microscopy; TEM, transmission electron microscopy; PrP, prion protein; FTIR, Fourier transform infrared; TFA, trifluoroacetic acid.

10.1021/bi047445a CCC: $30.25
Published on Web 02/26/2005

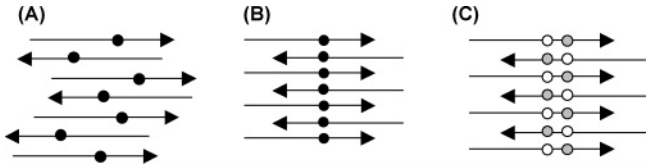

FIGURE 1: β-strands in H1. (A) depicts the unaligned form with the black circles representing A117. (B) and (C) show the aligned form where residue 117 (black circles in (B)) is aligned across the strands. In (C) residues 116 and 118 are highlighted as white and gray circles to show how labeling of these residues simultaneously will also result in $^{13}C{=}O$ coupling across the strands and give rise to the same decrease in $^{13}C{=}O$ band frequency as observed for labeling residue 117 alone.

Table 1: Derivatives of H1 Used in This Study[a]

name	sequence
H1	Ac-MKHMAGAAAAGAVV-NH_2
A117B	Ac-MKHMAGAABAGAVV-NH_2
A117G	Ac-MKHMAGAAGAGAVV-NH_2
A117V	Ac-MKHMAGAAVAGAVV-NH_2
A117L	Ac-MKHMAGAALAGAVV-NH_2
A117I	Ac-MKHMAGAAIAGAVV-NH_2
A117Z	Ac-MKHMAGAAZAGAVV-NH_2
A117U	Ac-MKHMAGAAUAGAVV-NH_2
A117X	Ac-MKHMAGAAXAGAVV-NH_2
H1 A117A*	Ac-MKHMAGAA**A**AGAVV-NH_2
H1**	Ac-MKHMAGA**A**A**A**GAVV-NH_2
A117B**	Ac-MKHMAGA**A**B**A**GAVV-NH_2
A117V*	Ac-MKHMAGAA**V**AGAVV-NH_2
A117G*	Ac-MKHMAGAA**G**AGAVV-NH_2
A117L*	Ac-MKHMAGAA**L**AGAVV-NH_2
A117I**	Ac-MKHMAGA**A**I**A**GAVV-NH_2
A117X**	Ac-MKHMAGA**A**X**A**GAVV-NH_2
(^{13}C)A116A A117L	Ac-MKHMAGA**A**LAGAVV-NH_2
A117L (^{13}C)A118A	Ac-MHKMAGAAL**A**GAVV-NH_2

[a] The bold lettering in the sequence indicates a residue labeled at the carbonyl with a ^{13}C. For simplicity, a single letter code for the synthetic amino acids is used, where B is aminobutyric acid (R = $-CH_2CH_3$), Z is norvaline (R = $-CH_2CH_2CH_3$), U is norleucine (R = $-CH_2CH_2CH_2CH_3$), and X is *tert*-leucine (R = $-C(CH_3)_3$).

we determine the conformation, strand alignment, and thermostability of the β-sheets formed in solution. Furthermore, using AFM, we have characterized the morphologies of the aggregates formed by these peptides. We find that the structure of the side chain at position 117 determines the strand alignment adopted within the β-sheets, and that peptides capable of adopting the same alignment as A117 H1 form stable β-sheet aggregates with a twisted fibril morphology. Other strand alignments produce aggregates which are disrupted by high temperature and which do not progress beyond formation of thin protofibril structures. The combination of isotope-edited IR, AFM, and systematic variation of the peptide allows the first detailed demonstration of the dictation of aggregate stability and morphology by the peptide structure and β-sheet organization.

MATERIALS AND METHODS

Peptide Synthesis. A series of peptides based on the H1 sequence (PrP(109−122)) were synthesized using standard Fmoc chemistry on a Pioneer peptide synthesizer (Table 1). Peptides were purified using reversed-phase HPLC (Pharmacia Biotech) and characterized by electrospray mass spectrometry. The peptides were then exchanged in 0.05 M DCl for 5 h to remove the trifluoroacetic acid (TFA) used to cleave the peptide from the solid-phase support resin (TFA absorbs at around 1674 cm^{-1} in the infrared and thus distorts the amide I′ band under investigation) and lyophilized overnight.

IR Measurements. Peptides were dissolved in a 1:1 mixture of acetonitrile and D_2O buffer (20 mM HEPES, 100 mM NaCl, pH 7.4; *13*) and vortexed until dissolution was complete. Concentrations used were approximately 15 mg/mL. IR measurements were taken using a Vector 22 FTIR spectrometer (Bruker) operating at a resolution of 4 cm^{-1}; the spectra were averaged over 512 scans. The IR cell was fitted with two CaF_2 windows separated by a 100 μm Teflon spacer. FTIR measurements were taken from 25 to 75 °C in steps of 10 °C, allowing 10 min at each temperature for the sample to reach equilibrium before the measurement was recorded. The temperature of the cell was controlled by a water jacket connected to an external water bath. The sample was then cooled back to 25 °C and maintained at that temperature until no further changes occurred in the IR spectra. In some cases, second and third heat/cool cycles were performed.

Data Analysis. Spectra were first scaled to the area of the 25 °C measurement for that peptide and then fitted globally to a three-band pseudo-Voigt function using a nonlinear least-squares (Levenberg−Marquardt) fitting routine (Microcal Origin). A pseudo-Voigt function is a commonly used simplification of a Voigt function which adds, rather than convolutes, Lorentzian and Gaussian functions (*19*). This results in the amide I′ band of each peptide being described by three overlapping bands, each one being the sum of a Gaussian and a Lorentzian band with equal widths at half the maximum height. The fit parameters employed by the routine allow the center frequency, area, width, and Gaussian/Lorentzian contributions for each band to be varied. For each peptide, the temperature-dependent spectra were fitted globally to allow the sharing of poorly defined parameters (for example, the width and position of the high-frequency β-sheet band, which has a very low intensity), thus decreasing uncertainty in their final value. The total area of the amide I′ band was used to determine the relative concentration; the amide I′ band areas in each case agreed within 10%. The sum of the areas of the two β-sheet bands was divided by the total area to determine the percentage of β-sheet.

Atomic Force Microscopy. Samples imaged (H1, A117G, A117B, A117I, A117L, A117V, and A117X) were initially dissolved in a 1:1 mixture of acetonitrile and D_2O buffer (20 mM HEPES, 100 mM NaCl, pH 7.4) to a concentration of 15 mg/mL. Samples of the stock solution were diluted 10-, 50-, and 100-fold immediately after preparation. A second set of dilutions was made after incubation of the stock for 2−5 days at 25 °C (to allow strands to adopt an equilibrium alignment). Dilution is necessary to disperse the aggregates sufficiently to allow comparison of the size and length to be made. AFM samples were made by immersing a small piece of freshly cleaved mica in the dilution for 15 s. The substrate was then rinsed with distilled water to remove any salts and any loosely bound peptide, air-dried, and affixed to a glass slide. The samples were imaged using a Digital Instruments Dimensions 3100 atomic force microscope, with an etched silicon probe, operating in the tapping mode using a scan rate of 1 Hz over a 2 μm × 2 μm area and 2 Hz over a 500 nm × 500 nm area.

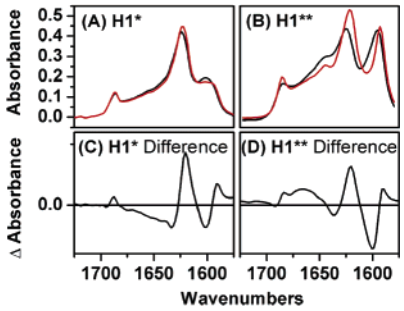

FIGURE 2: FTIR spectra of H1* (A) and H1** (B) at 25 °C before (black) and after (red) heating to 75 °C. Both spectra show a downshift in frequency of the ^{13}C band from 1601 to 1593 cm^{-1} demonstrating the β-strands aligning at residue 117. For H1* the shift is induced as ^{13}C-labeled residue 117 comes into register; for H1** the shift is induced by the ^{13}C label at residue 116 aligning with the ^{13}C label at residue 118 in the adjacent β-strand. (C) and (D) show the difference spectra (aligned − unaligned). Spectra were measured in a 1:1 mixture of acetonitrile and D_2O buffer (20 mM HEPES, 100 mM NaCl, pH 7.4).

RESULTS

Aligned and Unaligned H1 Aggregates Differ in Morphology. In peptides specifically ^{13}C labeled at a single backbone carbonyl, the frequency of the ^{13}C amide I′ band is a sensitive local probe of peptide secondary structure and the alignment of residues within a β-sheet. Due to transition dipole coupling, antiparallel β-sheets with labeled residues aligned and connected by interstrand hydrogen bonding have a ^{13}C amide I′ band about 10 cm^{-1} lower in frequency (at about 1592 cm^{-1}) compared to peptides with nonaligned labeled residues (*18*). Initially, the β-sheet formed by H1 is in a disordered, nonequilibrium arrangement, which converts to the equilibrium alignment slowly (τ > 10 h at 25 °C); the equilibrium alignment can also be reached by heating and then recooling the sample (*18*). This realignment is observed spectroscopically as a shift in the ^{13}C amide I′ band and is seen in Figure 2A for H1* (labeled at residue 117) and Figure 2B for the doubly ^{13}C labeled peptide H1**. As the peptides align, the ^{13}C amide I′ band at 1601 cm^{-1} (due to the misaligned form) decreases in intensity and the ^{13}C band at 1591 cm^{-1} (due to the aligned form) increases. In addition, the intensity of the ^{12}C amide I′ band increases and the intensity of the ^{13}C amide I′ band decreases upon strand alignment (Figure 2C,D); all of these spectral changes are consistent with ab initio models of IR spectra of isotopically labeled antiparallel β-sheets (*20*, *21*). These spectral changes, whether affected by heating/recooling or allowing the sample to stand at room temperature for extended periods of time, are not reversible; once aligned at residue 117, the β-sheet arrangement does not alter.

The morphologies of the H1 aggregates were characterized via AFM. Examples of images of H1 aggregates measured immediately after preparation of the stock solution (when the strands are not aligned) and after a 48 h incubation (after alignment is complete) are shown in Figure 3. The initial H1 sample contains a large number of smooth, thin protofibrils, with a height of ∼1.5 nm and a length of ∼100 nm (Figure 3A).[2] Some longer protofibrils of lengths >800 nm are also evident. They are similar in height to the shorter protofibrils and are curved, indicating their flexibility. The height of these protofibrils suggests that they are formed from a single chain of aggregated β-sheets, with side chains perpendicular to the mica surface. After 48 h, the aggregates are thicker (∼3 nm) and longer (the typical length being >800 nm) (Figure 3B), with a distinct beaded pattern. Characteristic examples of "smooth" and "beaded" aggregates are shown in Figure 4. The smooth versus beaded morphology of these fibrils is evident in the lengthwise cross-sectional slices along the fibrils; the beaded fibrils have a wavelike profile, with the height varying between ∼1.5 and 3 nm and a distance between crests of ∼100 nm (Figure 4C,D). The beaded fibrils are also straighter, indicating a greater degree of rigidity, and likely form from twisting together two of the chains of β-sheet aggregates.

Residue 117 Modulates Thermostability of β-Sheets. The alignment of residue 117 in all of the strands of the aggregate suggests that packing of the side chains at this position must be important to aggregate stability and conformation. To test this hypothesis, a series of peptides featuring substitutions at position 117 were prepared. The temperature-dependent FTIR spectra of each of the variants with an unbranched side chain at position 117, i.e., H1 (together with the 25 °C H1 spectrum deconvoluted into the two β-sheet bands and the random coil band), A117G, A117B, A117Z, and A117U, are shown in Figure 5. The characteristic signal for β-sheets, two sharp bands at around 1620 and 1690 cm^{-1}, is apparent in all samples. In the case of H1 and A117B (Figure 5A,D) the β-sheet bands can be clearly observed at all temperatures, suggesting the β-sheets formed are stable and highly resistant to melting. The A117G substitution results in a dramatic decrease in the amount of β-sheet present at 25 °C, and in this case the β-sheets can be completely melted by heating (Figure 5C).

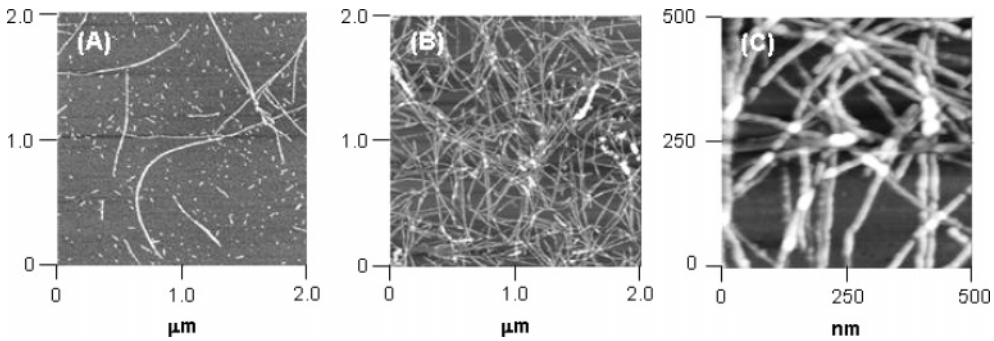

FIGURE 3: AFM images of H1 diluted 50× from stock solution immediately (A) and 2 days (B) after preparation. (C) shows the beaded nature of the fibrils in (B) at higher magnification. All images were measured in tapping mode, (A) and (B) at a scan rate of 1 Hz over an image area of 2 μm × 2 μm, (C) at a scan rate of 2 Hz over an image area of 500 nm × 500 nm.

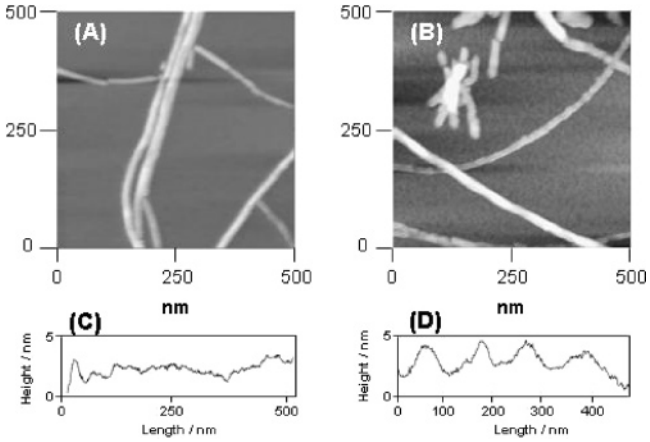

FIGURE 4: Typical AFM images of smooth and beaded fibrils. (A) shows A117L diluted 100-fold after 5 days of incubation, and (B) shows A117B diluted 10-fold. (C) and (D) show the height profiles of one fibril from A117L and A117B, respectively.

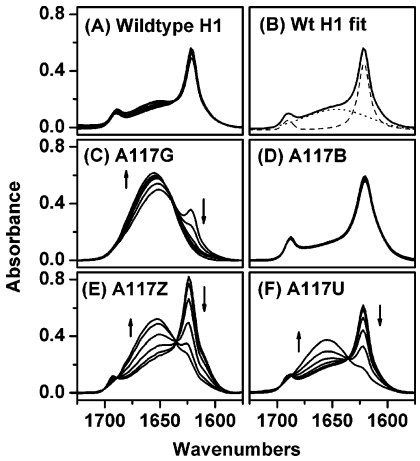

FIGURE 5: FTIR spectra of the H1 variants with a straight-chain side chain at position 117: wt H1 (plus the 25 °C spectrum deconvoluted into the two β-sheet bands and the random coil band, as determined by the fitting procedure), A117G, A117B, A117Z, and A117U. Spectra were recorded from 25 to 75 °C in 10 °C steps and have been normalized to the area of the 25 °C measurement for that peptide.

To quantify the β-sheet content (percentages of the total number of residues in the sample which adopt a β-sheet conformation) of each sample at each temperature, the amide I′ spectra of H1 were fit to a three-band pseudo-Voigt fit function. For each peptide, the amide I′ peak was found to be comprised of three bands at approximately 1620, 1690, and 1650 cm^{-1}. The bands at 1620 and 1690 cm^{-1} are ascribed to the antiparallel β-sheet structure in accordance with previous assignments from the literature (*13*,*19*) and with ab initio calculations (*23*). The final band is attributed to random coil with possibly some α-helical contribution; this third band is broader and more Gaussian shaped than the other two, which supports the assignment of this band to a less ordered structure.

Results of the spectral fits are summarized in Table 2. The H1 sample contains 42% β-sheet at 25 °C and 41% β-sheet at 75 °C. After cooling of the sample to 25 °C, the amount of β-sheet increases to 47%. The results for A117B show that the β-sheet configuration accounts for 80% of the structure at 25 °C, and is largely unchanged upon heating to 75 °C and recooling to 25 °C (Figure 5D). For side chains longer than $-CH_2CH_3$, the percentage of β-sheet detected at 25 °C decreases compared to that for the shorter side chains, and the β-sheets of these variants melt upon heating to 75 °C (Figure 5E,F).

[2] The width of fibrils in AFM is influenced by the shape and width of the AFM tip. Absolute height measurements are still affected by the electrostatic environment and nature of the substrate materials, but relative measurements (i.e, comparisons of one fibril to another) are quite valuable (*7*, *22*).

Table 2. Results of the Pseudo-Voigt Fits to the Temperature-Dependent FTIR Spectra of All H1 Variants[a]

	% β-sheet		
peptide	25 °C, initial	75 °C	25 °C, final
H1	41.8	41.3	47.1
A117B	80.1	83.7	84.3
A117G	12.4	0	
A117V	60.9	11.8	59.8
A117L	51.2	3.0	48.1
A117I	71.1	47.0	81.6
A117Z	52.6	7.1	50.5
A117U	47.6	7.4	40.9
A117X	52.4	30.5	67.5

[a] The "final" 25 °C measurement was taken after the sample was cooled from 75 °C and any re-formation of β-sheet was complete.

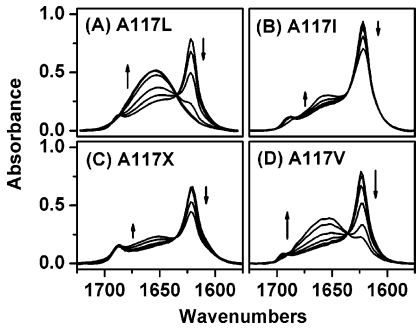

FIGURE 6: FTIR spectra of the H1 variants with a branched side chain at position 117, A117L, A117I, A117X, and A117V. Spectra were recorded from 25 to 75 °C in 10 °C steps and have been normalized to the area of the 25 °C measurement for that peptide.

Spectra of peptides with branched side chains (A117L, A117I, A117X, and A117V) are shown in Figure 6. In the spectra of A117L and A117V (Figure 6A,D), the β-sheet bands disappear almost entirely upon heating to 75 °C but re-form upon cooling back to 25 °C. A117I and A117X (Figure 6B,C) retain a large amount of β-sheet structure at high temperatures, and the spectra of the recooled samples have a larger percentage of β-sheet than the initial 25 °C spectra. A117L, A117I, and A117X each have more β-sheet than the variant with a straight chain $-C_4H_9$ side chain (A117U) with 51%, 71%, and 52% β-sheet, respectively, compared with 48% β-sheet reported for A117U at 25 °C. The same is also true for the branched (A117V, 62% β-sheet at 25 °C) and unbranched (A117Z, 53% β-sheet at 25 °C) $-C_3H_7$ side chain.

Residue 117 Also Modulates Strand Alignment. Isotope-edited spectra reveal that A117B and A117I adopt an equilibrium structure similar to that of the wild-type H1, with residue 117 fully aligned. The ^{13}C low-frequency β-sheet band of A117B** is found at 1592 cm^{-1} immediately after dissolution and does not move throughout a heat−cool cycle, indicating that the peptide immediately adopts the favored

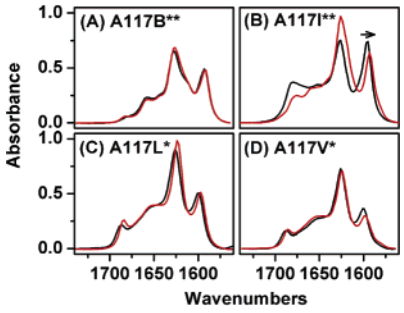

FIGURE 7: FTIR spectra of A117B**, A117I**, A117L*, and A117V* at 25 °C before (black) and after (red) heating to 75 °C. The ^{13}C band of A117B** remains at 1592 cm^{-1} throughout the anneal, but the same heat−cool process causes the ^{13}C band of A117I** to shift from 1596 to 1593 cm^{-1} as the peptide aligns. In the case of A117L* and A117V* the ^{13}C band shifts to 1597 and 1599 cm^{-1}, respectively, following the anneal.

aligned conformation (Figure 7A). As with H1, the ^{13}C amide I′ band of A117I** shifts to ∼1593 cm^{-1} with heating or prolonged time periods (Figure 7B). The ^{13}C amide I′ band of A117X** also undergoes a large shift after annealing (data not shown).

A117V* and A117L*, on the other hand, adopt a β-sheet alignment different from that of H1 (Figure 7C,D). In the case of A117L*, the ^{13}C amide I′ band shifts only 3 cm^{-1} to 1597 cm^{-1} after annealing, indicating some increased ordering of the system but not alignment at position 117. Labeling residue 118 of A117L results in a ^{13}C amide I′ band frequency identical to that of the A117L* peptide, and labeling residue 116 causes the ^{13}C band to appear at 1599 cm^{-1}; none of these positions are aligned within the β-sheet structure. For A117V*, the ^{13}C amide I′ band appears at 1599 cm^{-1} after annealing (also a 2−3 cm^{-1} shift).

On the basis of the spectra of isotope-labeled peptides, A117B, A117I, and A117X all adopt the same strand alignment as the wild-type H1, while A117L and A117V adopt a different arrangement. These alignment results correlate with the thermostability observations made above; all of the peptides which adopt the same alignment as H1 resist unfolding upon an increase in temperature, while the peptides which adopt a different alignment scheme go from β-sheet to random coil upon heating to 75 °C. Moreover, in the cases where the β-strands align at residue 117 after annealing (H1, A117I, and A117X), the total β-sheet content increases after recooling to 25 °C; in cases where no alignment at residue 117 occurs the second 25 °C spectrum shows a less intense β-sheet signal than was observed initially. Thus, the aligned conformation is lower in energy (more favored at 25 °C) than the misaligned conformation.

Morphology Differences as a Function of Residue 117. The aggregates formed by the different H1 variants also show differences in aggregate morphology as imaged by AFM. Example images are shown in Figure 8. A117I and A117B produce long (>2 μm) beaded fibrils (height 3−4 nm) after prolonged incubation at room temperature, similar to the aligned H1 (Figure 8A illustrates this for the case of A117I; beaded fibrils of A117B can be seen at higher magnification in Figure 4B). The majority of the fibrils observed in these samples were rigid and straight. A117V and A117L, on the other hand, only form thin, smooth protofibrils even after prolonged incubation (height of ∼2 nm for A117L and A117V), similar to the unaligned H1 (Figure 8B illustrates

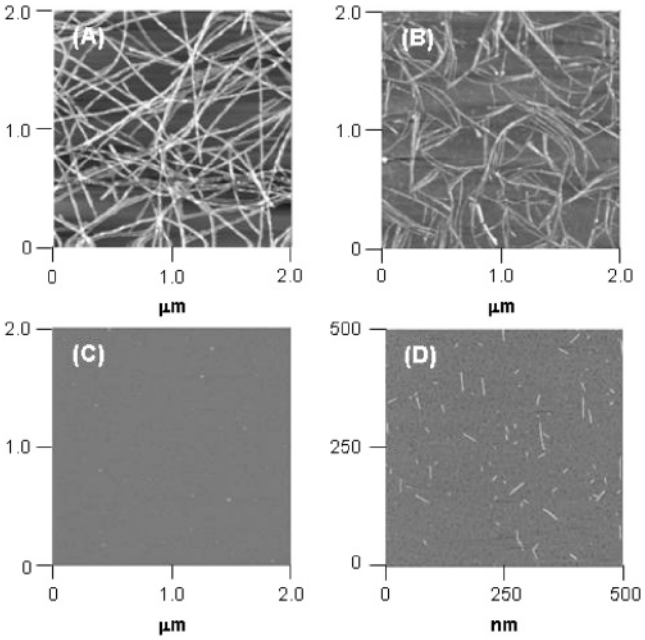

FIGURE 8: AFM images of (A) A117I, showing the beaded nature of fibrils observed after the β-strands have aligned, (B) A117V showing smooth, flexible protofibrils, (C) A117G showing how no protofibrils form in this H1 variant, and (D) A117V after heating of the sample used to prepare image B to 75 °C, showing the disrupted protofibrils. All samples were diluted 100-fold, and images were measured in tapping mode, (A)−(C) at a scan rate of 1 Hz over an image area of 2 μm × 2 μm, (D) at a scan rate of 2 Hz over an image area of 500 nm × 500 nm.

this for the case of A117V; smooth fibrils of A117L can be seen at higher magnification in Figure 4A). Both of these peptides form long curved fibrils indicative of greater flexibility. Samples of A117G had no protofibrils or fibrils present (Figure 8C). Heating the samples of A117V and A117L to 75 °C before deposition onto mica disrupted the long thin protofibrils present at 25 °C, with only a few short, thin protofibrils with lengths of 50−100 nm and heights of ∼2 nm observed (Figure 8D for the case of A117V).

DISCUSSION

Relationship between Alignment and Aggregate Morphology. H1 forms twisted fibrils only after the alignment of β-sheets at residue 117; the aggregates formed initially (when the strands are not aligned) consist only of thin protofibrils. Similar relationships between strand alignment and aggregate morphology are observed for A117B, A117I, A117X, A117L, and A117V; peptides that adopt the same equilibrium alignment as H1 form twisted fibrils, while peptides that adopt different alignments form only thin protofibrils. Attaining an ordered, thermodynamically favored arrangement of strands within a β-sheet is a prerequisite to forming higher order aggregate structures, and the process of alignment is likely a key (perhaps rate-determining) step in the fibril nucleation process. The structure of the protofibril consisting of β-sheets with proper alignment enables the twisting together of two protofibrils to form thicker, more rigid fibrils.

Effect of Residue 117 on β-Sheet Formation. Moreover, these results also suggest a general mechanism by which site-specific amino acid substitutions can affect the kinetics of fibril formation. In the H1 peptides, substitutions that prevent

the peptide from adopting the ordered alignment also arrest aggregate formation at the protofibril stage, inhibiting the formation of larger (and more stable) twisted fibrils. In other words, *peptide structure determines aggregate alignment, which in turn determines fibril morphology*. Not only may this scheme be valuable for understanding other aggregating peptide systems, it also suggests a strategy for designing peptide or peptidomimetic inhibitors capable of arresting aggregate formation at different stages.

Dissecting the Relationship among Peptide Structure, Strand Alignment, and Thermostability. Small differences in the structure of the side chain at position 117 have strikingly large effects on the aggregates formed. For example, the A117L peptide does not adopt the same alignment as H1, forms aggregates which melt at high temperatures, and gives rise to smooth protofibrils; A117I, on the other hand, adopts the 117 alignment, forms thermostable aggregates, and gives rise to twisted fibrils. Clearly, the properties of H1 are very sensitive to the structure of the side chain at position 117, and close comparison of a series of peptides in which the structure of residue 117 is systematically varied illustrates how single mutations may alter the energy landscape for peptide aggregation.

H1 is initially kinetically trapped in a misaligned β-sheet structure; heating (or waiting for an extended time at 25 °C) allows it to adopt a lower energy, aligned conformation. When alanine 117 is substituted for aminobutyric acid (A117B, extending the side chain at position 117 by one $-CH_2-$ unit), the peptide immediately adopts a β-sheet structure with position 117 aligned; in other words, the A117B substitution eliminates the kinetic trap observed with H1. The A117B peptide is also thermostable up to 75 °C, and the percent β-sheet measured ($\sim$80%) is about the maximum to be expected for the structure shown in Figure 1 (with about 11 of the 14 residues participating in the β-sheet core). Thus, the aligned conformation of the A117B peptide is significantly lower in energy than either the misaligned β-sheet or the dissociated, random coil state (neither of which are observed, even at high temperatures). The longer side chain likely increases van der Waals interactions between strands within the β-sheet, resulting in a more stable aligned structure and a lower barrier to alignment than observed with H1.

Linearly extending the carbon chain of the side chain of residue 117 beyond two carbon units, as in norvaline (A117Z) and norleucine (A117U), results in β-sheets which are not thermostable (β-sheets melting completely upon heating to 75 °C), and do not align at position 117 upon recooling. Because these peptides melt at higher temperatures, either the energy difference between the β-sheet and random coil states is smaller or the barrier between these states is lower than in A117B. The lack of alignment indicates that either the 117 aligned state is higher in energy than the misaligned state or the barrier to alignment is significantly higher than in H1 or A117B. While the longer chains should increase van der Waals interactions between strands, these side chains will also undergo a significant loss of side chain entropy when packed across from each other in a β-sheet, as this restricts the number of available conformations to just one compared to the numerous rotameric states available in an unstructured protein (*24*).

Interestingly, straight-chain norleucine at position 117 (A117U) forms less β-sheet than leucine (A117L), isoleucine (A117I), or *tert*-leucine (A117X) at that position; similarly, norvaline at position 117 (A117Z) forms less β-sheet than the peptide with valine at 117 (A117V). These differences also arise from the loss of side chain entropy upon side chain packing (*25*). A117L and A117V do not adopt the aligned conformation, while A117I and A117X do. The shape of the side chain at position 117 may effect the energy barrier to strand realignment, kinetically trapping the A117L and A117V in the misaligned conformation. This also traps the aggregates in the smooth protofibril morphology; in this case, the barrier between the aligned and misaligned β-sheets is also the rate-determining barrier between the smooth protofibril and twisted fibril morphologies.

Shortening the side chain at position 117 by replacing alanine with glycine (A117G) disrupts β-sheet formation. Glycine residues typically introduce greater backbone flexibility into polypeptide chains, disrupting ordered secondary structure by introducing kinks into the backbone. Introduction of a glycine at position 117 thus destabilizes the extended β-sheet conformation, even at low temperatures.

Conclusions. The formation of twisted bundles of fibrils by the peptide H1 depends on the organization of the β-strands within the aggregate. Single amino acid substitutions can change the relative stabilities of the aligned, misaligned, and random coil conformations, as well as the kinetic barrier between the aligned and misaligned states. While these studies are on a small peptide system in a water/acetonitrile solution, the adoption of a stable arrangement of strands within a β-sheet aggregate may be a general feature of the mechanism of fiber formation for polypeptides, a molecular-level rearrangement which occurs during the "nucleation" phase of aggregation. The observation that specific side chain interactions modulate this process suggests that fiber formation can be arrested at different phases by designed peptides or peptidomimetics.

ACKNOWLEDGMENT

The pseudo-Voigt fit function was written and supplied by Dr. Martin Volk, University of Liverpool, U.K.

REFERENCES

1. Dobson, C. M. (2003) Protein-misfolding diseases: Getting out of shape, *Nature 426*, 884−890.
2. Prusiner, S. B. (1991) Molecular biology of prion diseases, *Science 252*, 1515−1522.
3. Scherzinger, E., Lurz, R., Turmaine, M., Mangiarini, L., Hollenbach, B., Hasenbank, R., Bates, G. P., Davies, S. W., Lehrach, H., and Wanker, E. E. (1997) Huntingtin-encoded polyglutamine expansions form amyloid-like protein aggregates in vitro and in vivo, *Cell 90*, 549−558.
4. Fandrich, M., Fletcher, M. A., and Dobson, C. M. (2001) Amyloid fibrils from muscle myoglobin, *Nature 410*, 165−166.
5. Walsh, D. M., Hartley, D. M., Kusumoto, Y., Fezoui, Y., Condron, M. M., Lomakin, A., Benedek, G. B., Selkoe, D. J., and Teplow, D. B. (1999) Amyloid β-protein fibrillogenesis, *J. Biol. Chem. 274*, 25945−25952.
6. Serpell, L. C., Blake, C. C. F., and Fraser, P. E. (2000) Molecular structure of a fibrillar Alzheimer's aβ fragment, *Biochemistry 39*, 13269−13275.
7. Goldsbury, C., Kistler, J., Aebi, U., Arvinte, T., and Cooper, G. J. S. (1999) Watching amyloid fibrils grow by time-lapse atomic force microscopy, *J. Mol. Biol. 285*, 33−39.

8. Huang, T. H. J. Yang, D−S., Fraser, P. E., and Chakrabartty, A. (2000) Alternate aggregation pathways of the Alzheimer β-amyloid peptide. An in vitro model of preamyloid, *J. Biol. Chem. 275*, 36436−36440.
9. Harper, J. D., Wong, S. S., Lieber, C. M., and Lansbury, P. T. (1997) Atomic force microscopic images of seeding fibril formation and fibril branching by the Alzheimer's disease amyloid-β protein, *Chem. Biol. 4*, 419−425.
10. Makin, O. S., and Serpell, L. C. (2004) Structural characterisation of islet amyloid polypeptide fibrils, *J. Mol. Biol. 335*, 1279−1288.
11. Serpell, L. C., and Smith, J. M. (2000) Direct visualisation of the β-sheet structure of synthetic Alzheimer's amyloid, *J. Mol. Biol. 299*, 225−231.
12. Gasset, M., Baldwin, M. A., Lloyd, D. H., Gabriel, J.-M., Holtzman, D. M., Cohen, F. E., Fletterick, R., and Prusiner, S. B. (1992) Predicted α-helical regions of the prion protein when synthesized as peptides form amyloid, *Proc. Natl. Acad. Sci. U.S.A. 89*, 10940−10944.
13. Nguyen, J., Baldwin, M. A., Cohen, F. E., and Prusiner, S. B. (1995) Prion protein peptides induce α-helix to β-sheet conformational transitions, *Biochemistry 34*, 4186−4192.
14. Conway, K. A., Harper, J. D., and Lansbury, P. T. (2000) Fibrils formed in vitro from α-synuclein and two mutant forms linked to Parkinson's disease are typical amyloid, *Biochemistry 39*, 2552−2563.
15. Halverson, K., Sucholeiki, I., Ashbury, T. T.,and Lansbury, P. T. (1991) Location of β-sheet-forming sequences in amyloid proteins by FTIR, *J. Am. Chem. Soc. 113*, 6701−6703.
16. Laws, D. D., Bitter, H.-M., Liu, K., Ball, H. L., Kaneko, K., Wille, H., Cohen, F. E., Prusiner, S. B., Pines, A., and Wemmer, D. E. (2001) Solid-state NMR studies of the secondary structure of a mutant prion protein fragment of 55 residues that induces neurodegeneration, *Proc. Natl. Acad. Sci. U.S.A. 98*, 11686−11690.
17. Brown, D. R. (2000) Altered toxicity of the prion protein peptide PrP(106−126) carrying the ala117 → val mutation, *Biochem. J. 346*, 785−791.
18. Silva, R. A. G. D., Barber-Armstrong, W., and Decatur, S. M. (2003) The organization and assembly of a β-sheet formed by a prion peptide in solution: an isotope-edited FTIR study, *J. Am. Chem. Soc. 125*, 13674−13675.
19. Chirgadze, Y. N., Shestopalov, B. V., and Venyaminov, S. Y. (1973) Intensities and other spectral parameters of infrared amide bands of polypeptides in the β- and random forms, *Biopolymers 12*, 1337−1351.
20. Brauner, J. W., Dugan, C., and Mendelsohn, R. (2000) ^{13}C isotope labeling of hydrophobic peptides. origin of the anomalous intensity distribution in the infrared amide I spectral region of β-sheet structures, *J. Am. Chem. Soc. 122*, 677−683.
21. Kubelka, J., and Keiderling, T. A. (2001) The anomalous infrared amide I intensity distribution in 13c isotopically labeled peptide β-sheets comes from Extended Multiple-Stranded Structures. An ab initio study, *J. Am. Chem. Soc. 123*, 6142−6150.
22. Muller, D. J., and Engel, A. (1997) The height of biomolecules measured with the atomic force microscope depends on electrostatic interactions, *Biophys. J. 73*, 1663−1644.
23. Kubelka, J., and Keiderling, T. A. (2001) Differentiation of β-sheet-forming structures: Ab initio-based simulations of IR absorption and vibrational CD for model peptide and protein β-sheets, *J. Am. Chem. Soc. 123*, 12048−12058.
24. Doig, A. J., and Sternberg, M. J. E. (1995) Side-chain conformational entropy in protein folding, *Protein Sci. 4*, 2247−2251.
25. Creamer, T. P. and Rose, G. D. (1992) Side-chain entropy opposes α-helix formation but rationalizes experimentally determined helix-forming propensities, *Proc. Natl. Acad. Sci. U.S.A. 89*, 5937−5941.

BI047445A